Nanoscale

Nanonet-Nano Fiber Electrospun Mesh of PCL-Chitosan for Controlled and Extended Release of Diclofenac Sodium

Journal:	*Nanoscale*
Manuscript ID	NR-ART-08-2020-005968.R1
Article Type:	Paper
Date Submitted by the Author:	18-Sep-2020
Complete List of Authors:	Saudi, Sheikh; North Carolina Agricultural and Technical State University College of Engineering, Nanoengineering Bhattarai, Shanta; North Carolina Agricultural and Technical State University College of Arts and Sciences Adhikari, Udhab; North Carolina Agricultural and Technical State University College of Engineering Khanal, Shalil; North Carolina Agricultural and Technical State University College of Arts and Sciences Sankar, Jagannathan; North Carolina Agricultural and Technical State University College of Engineering, Mechanical Engineering Aravamudhan, Shyam; North Carolina Agricultural and Technical State University Bhattarai, Narayan; North Carolina Agricultural and Technical State University College of Engineering, Chemical, Biological and Bioengineering

Nanonet-Nano Fiber Electrospun Mesh of PCL-Chitosan for Controlled and Extended Release of Diclofenac Sodium

Sheikh Saudi [a,g], Shanta R Bhattarai [b,c], Udhab Adhikari [d,g], Shalil Khanal [e,g], Jagannathan Sankar [d,g], Shyam Aravamudhan [a] , Narayan Bhattarai [f,g] *

[a] Department of Nanoengineering, Joint School of Nanoscience and Nanoengineering, North Carolina A&T State University, Greensboro, NC 27401, USA

[b] Department of Chemistry and Department of Biology, North Carolina A&T State University, Greensboro, NC 27411, USA

[c] Department of Biological Science, Winston-Salem State University, Winston-Salem, NC 27110, USA

[d] Department of Mechanical Engineering, North Carolina A&T State University, Greensboro, NC 27411, USA

[e] Department of Applied Science and Technology, North Carolina A&T State University, Greensboro, NC 27411, USA

[f] Department of Chemical, Biological, and Bioengineering, North Carolina A & T State University, Greensboro, NC 27411, USA

[g] NSF-ERC for Revolutionizing Metallic Biomaterials, North Carolina A&T State University, Greensboro, NC 27411, USA

* *Corresponding Author: N Bhattarai (**nbhattar@ncat.edu**)*

Abstract: Nanonet-Nano Fiber Electrospun Mesh

Electrospun nanofiber (EN) technology has been used in the past to generate electrostatically charged multilayer-nanofibers. This platform offers versatile applications including in tissue engineering, drug delivery, wound dressings, and high-efficiency particulate air filters. In this study, we synthesized for the first time a nanonet-nanofiber electrospun meshes (NNEMs) of polycaprolactone (PCL)-chitosan (CH) using EN technology. The fabricated NNEMs were utilized for high payload delivery and controlled release of a water-soluble drug. Diclofenac Sodium (DS), the hydrophilic-anti-inflammatory drug was selected as a model drug because of its high aqueous solubility and poor compatibility with insoluble polymers. Various compositions of DS drug-loaded NNEMs (DS-NNEMs) were synthesized. Physicochemical properties such as structure, morphology, aqueous stability, and chemical properties of DS-NNEMs were evaluated. High drug entrapment efficiency and concentration-dependent drug release patterns were investigated for up to 14 days. Furthermore, the biocompatibility of the DS-NNEMs was tested with NIH 3T3 cells. The physicochemical characterization results showed that DS drug is a key contributing factor in the generation of nanonet-nanofiber networks during electrospinning. DS-NNEMs also enhanced 3T3 cell adhesion, viability, and proliferation in the nanonet-nano fiber network through the controlled release of DS. The presented EN technology-based biodegradable NNEMs material is not only limited for the controlled release of hydrophilic-anti-inflammatory drugs but also can be a suitable platform for loading and release of antiviral drugs.

Introduction:

Electrospinning technology has been known for the last several years as an established and cost-effective technique to produce small-diameter polymer fibers ranging from several nanometers to micrometers with controlled surface morphology. Electrospun nanofibers are employed in engineering fields including filtration [1-3], masking/fabrics [4, 5], sensors [6, 7], and energy-related applications, etc. [8]. Biodegradable polymeric nanofibrous materials generated by several researchers including our research group using the electrospinning technique [9-12] have been investigated extensively in biomedical fields particularly in drug delivery and tissue engineering [13-19]. Special features such as biodegradable fibrous mesh structures, highly porous and interconnected networks, and large surface to volume ratio [20-23] of the fibers have been utilized to increase the interaction of the material surface with biomolecules and cells [24, 25].

In recent years, several remarkable properties of the electrospun fibers have been tuned by changing the architecture of nanofiber assembly and chemistry of the materials. Adding extra ultra-fine architectures in the conventional electrospun nanofibers such as beaded nanofiber nets and spider nano-nets, called thereafter as nanonet-nanofiber-electrospun mesh (NNEM), can offer a versatile fibrous material platform for high-performance applications. Ding et al., group [26-28], as well as other researchers [29-31], have developed varieties of nanonet fibrous membranes for unique applications such as air filtration [26-31]. When a high voltage is applied to an electrospunable polymer solution containing ionic complexes and droplets of charged particles or soluble salts, the Taylor cone undergoes stretching and solvent evaporation process, which results nano-net structured fibers [26, 27]. Nanonets of polyvinyl alcohol (PVA), polyamide-6 (PA-6),

polyurethane (PU), polyacrylonitrile (PAN), and Poly (*m*-phenylene isophthalamide) (PMIA), poly (acrylic acid), etc. have been synthesized to exhibit several desired functions [26-31].

We are particularly interested in NNEMs of biodegradable and biocompatible polymers that can mimic nanofibrillar architectures of Extracellular Matrix (ECM). In addition, the complexity of nanonet nanofibers with significant advantages offers several applications including air/water filters, sensors, smart textiles, biocompatible scaffolds for tissue engineering, and drug delivery. We synthesized for the first time a NNEM of polycaprolactone (PCL)-chitosan (CH)- diclofenac sodium (DS) electrospun mesh membrane. DS played a critical role in the production of nano-net structures of PCL-CH. DS also served as a model drug to study release characteristics and the toxicity effect of DS-NNEM. DS is a non-steroidal anti-inflammatory drug (NSAID) [32], which exerts analgesic and anti-inflammatory impacts by inhibiting the cyclooxygenase enzyme family. DS is also known for relieving pain caused by rheumatoid arthritis, migraines, or menstrual pain [33, 34]. In this study, DS also played a critical role in the production of nano-net structures of PCL-CH.

Both PCL and CH are well-known polymers used in controlled drug delivery and tissue engineering applications [35]. PCL, a semi-crystalline linear polyester has good properties such as high flexibility [36], slow biodegradability [37], low melting point (60^{o}C) [38], release of non-toxic byproducts in degradation [35, 39, 40] and has Food and Drug Administration (FDA) approval for medical device applications [39]. The broader application of PCL in tissue engineering and drug delivery field has a drawback because of its slow degradation rate and lack of cell affinity *in vivo* due to its high crystallinity and hydrophobicity [41]. It has been reported that the biodegradability and biocompatibility of PCL can be enhanced by copolymerizing [42] or blending with a variety of other polymers [43, 44]. One such promising polymer is CH [35], a N-

deacetylated derivatives of chitin [36]. CH, a naturally occurring polymer, derived from the exoskeletons of crustaceans, is biodegradable, biocompatible, non-toxic, antimicrobial, and resembles the structure of glucosamine glycan (GAG), a major component of ECM [11, 16, 45].

In this study, we synthesize DS-NNEMs by electrospinning the PCL-CH solutions with different amounts of DS. We evaluate different physicochemical properties such as structure, morphology, aqueous stability, and drug entrapment and release patterns of the DS-NNEMs. We tested our hypothesis that DS plays a major role in the formation of the ultrafine nano-net structures, alters the drug release rate, and suppresses the drug toxicity to fibroblast cells *in vitro* [46, 47]. DS-NNEMs studies with different compositions exhibit that the biomimetic nano-net nanofiber meshes can be potentially used to deliver biologically active therapeutics over a long period.

Materials and Methods

Materials*:* PCL (Mn 80 kDa), chitosan (CH) (Medium molecular weight; Lot # STBF3507V) and diclofenac sodium (DS) salt were purchased from Sigma Aldrich (Millipore Sigma; Saint Louis, MO). 2,2,2-trifluoroethanol (TFE) and dichloromethane (DCM) was obtained from Alfa Aesar (Ward Hill, MA). 2,2,2-trifluoroacetic acid (TFA) was purchased from ACROS Organics (New Jersey, USA). Dulbecco's phosphate-buffered saline (DPBS), and Dulbecco's modified Eagle's medium (DMEM) were obtained from Life Technologies (Grand Island, NY, USA). Alamar Blue and Lactate Dehydrogenase (LDH) assay kit was purchased from Thermo-scientific (Waltham, MA, KY).

Solution preparation*:* The PCL solutions were prepared at a concentration of 12% (w/w) in TFE, CH solutions at 6% (w/w) in TFA/DCM (70:30, v/v). DS was loaded to CH solution in a

concentration of 0 to 3 wt% compared to the amount of CH. To make a homogeneous dispersion, the DS was added to the solvent first, and CH was added afterward. Both PCL and CH-DS solutions were stirred with a magnetic bar overnight. Immediately before electrospinning, PCL and CH-DS solutions were prepared at a ratio of 60:40. The proportion of the solid components were adjusted in such a way that the resulting fiber composition will have PCL-CH ratio 70:30 (w/w) and concentration of DS will be 0 to 12% (w/w) (0 to 12 weight % DS loaded samples are represented by PC-0, PC-4, PC-8, and PC-12) of the total polymer weight in the solutions (Table 1). The mixed solutions were properly vortexed for homogeneous blend and transferred to an ultrasonic bath (PS-10A Jeken ultrasonic cleaner bath, China) for 5 minutes to get rid of any air bubble.

Table 1: DS-NNEMs sample designation and composition

DS-NNEMs	Composition ratio (PCL: CH-DS)	Proportion of PCL: chitosan (w:w)	% of DS (w/w)
PC-0	60:40	70:30	0
PC-4	60:40	70:30	4
PC-8	60:40	70:30	8
PC-12	60:40	70:30	12

Electrospinning of DS-NNEMs*:* Electrospinning was carried as described in our previous publications [10, 48]. Briefly, the electrospinning setup consisted of a syringe pump (Model 78-01001, Fisher Scientific, Pittsburgh, PA, USA), a high-voltage power supply (Model

CZE100PN30, Spellman High Voltage Electronics Corporation, Hauppauge, NY, USA) and a collector drum. Approximately 7 mL of the PCL-CH solution with different amounts of DS was placed in a 10 mL syringe with an attached 18G-diameter hypodermic needle. The syringe tip was placed approximately 10 cm from the collector, and 15 kV voltage supply was used to charge the solution. The feeding rate of the solution was precisely controlled by the syringe pump system, which was adjusted to a flow rate of 0.5-0.9 mL/h. The solution was spun towards the rotating grounded drum (200 rpm) wrapped with aluminum foil. After performing the electrospinning, the *DS-NNEMs* were allowed to dry overnight in a chemical hood and were detached from the aluminum foil for physical, chemical, and biological characterization. The *DS-NNEMs* were neutralized with 14% ammonium hydroxide for 5 min, followed by rinsing with DI water three times and lyophilized (FreeZone 2.5 Liter Benchtop Freeze Dry System, Labconco, Kansas City, MO, USA) for 2 h.

Surface morphology analysis of DS-NNEMs*:* Surface morphology of all *DS-NNEMs* samples were analyzed by Scanning Electron Microscope (SEM; Zeiss Auriga FIB/FESEM, Carl Zeiss Microscopy, LLC, NY, USA). Briefly, *DS-NNEMs* samples were cut, attached to copper tape and sputter-coated with gold-palladium using a coating system (Leica EM ACE200, IL, USA) for 30 seconds (coating depth = 5 nm) at 15 mA. SEM images were taken at an accelerating voltage of 3 kV. The size distribution of the fiber in *DS-NNEMs* samples was analyzed through SEM images with the use of ImageJ software (NIH, Bethesda, MD, USA). Diameter length was converted to pixels with the help of a scale bar. Fifty individual fibers of *DS-NNEMs* from each group (n = 3) of SEM images were measured in pixels. The average size and standard deviation were calculated based on converted ImageJ data.

***FTIR analysis**:* Fourier-transform infrared spectroscopy (FTIR) was used to identify functional groups and the presence of each component of fiber materials in the meshes. FTIR spectra were obtained with a Varian 670 FT-IR Spectrophotometer (Varian, Inc., Palo Alto, CA, USA) in the range of 4000 to 400 cm^{-1}. FTIR spectra were recorded with 64 scans at a resolution of 4 cm^{-1}.

***Differential scanning calorimetry (DSC) analysis**:* Differential scanning calorimetry (DSC) analysis was carried out using a DSC Q200 differential scanning calorimeter (TA Instruments Co., USA). All analyses were performed with a ~5 mg sample placed in standard aluminum pans under the nitrogen environment (40 mL/min). Sealed samples were heated at 10 °C/min from 20 to 160 °C. Melting temperature (T_m) was measured from the first scan peak. Degree of crystallinity was evaluated by the following equation,

$$X_c = \frac{\Delta H_m}{\Delta H_0} \times 100\% \quad (1)$$

where X_c is the degree of crystallinity, ΔH_m is the enthalpy of melting for the samples and $\Delta H_o$is the melting enthalpy for 100% crystalline PCL which was taken as 139.5 J/g [49].

Mechanical properties: Mechanical properties of the *DS-NNEMs* were characterized using a uniaxial testing machine (Instron 5542, Canton, MA, USA) with a 500-N load cell under a crosshead speed of 4 mm/min. Samples were cut in a rectangular form of dimension 14 mm × 5mm × *T*, where *T* is the thickness. The thickness of the *DS-NNEMs* was taken in three different locations with a Digimatic micrometer for all trials. Samples were fixed with a custom-designed rectangular template of dimension 40 mm × 10 mm [10]. Young's modulus and the tensile strength of the *DS-NNEMs* were measured from the strain-stress curve. Five specimens per mesh type were tested.

Water contact angle test: Wettability of the *DS-NNEMs* was analyzed by measuring static contact angle with a Goniometer OCA 15 (Data Physics, Charlotte, NC, USA) analyzer. A drop of deionized water was dropped onto the surface of *DS-NNEMs* by using a micro syringe attached with a needle. A picture of the drop was taken in three different time points (0, 10, and 20 sec) after the drop set on to the sample. The contact angle was calculated by analyzing the shape of the drop by DROPimage advanced (Ramé-hart instrument co., NJ, USA). Three samples for each group were tested to calculate the average value. All measurements were taken at room temperature.

***In-vitro release of DS drug from DS-NNEMs*:** To investigate the release of DS from all *DS-NNEMs*, samples pieces (3 cm × 3 cm) were attached to the coverslip (n=3, per mesh type), using a biocompatible silicone-based elastomeric glue (Kwik-Sil™, Sarasota, FL, USA). These samples were incubated in a 50 mL conical tube with 25 mL of 1× Dulbecco's phosphate-buffered saline (DPBS) solution and placed in a shaking water bath (Dubnoff Shakebath-2876, Thermo Fisher Scientific, Fair Lawn, NJ, USA) at 37 °C and 50 rpm for 14 days. At various time intervals, 5 mL of solution was extracted, and the medium in the tube was replenished with 5 mL of fresh 1× DPBS. The absorbance of each solution was measured by using a UV-Spectrophotometer (CLARIOstar Plus, BMG LABTECH Inc., Cary, NC, USA) at 277 nm wavelength and compared with the standard calibration curve (**Supplemental Information SI-1**) to determine the amount of drug release. All experiments were performed in triplicates.

Cell preparation: NIH-3T3 cells, mouse fibroblast cell lines were purchased from the American Tissue Type Culture Collection (ATCC 1658, Manassas, VA). The cells were cultured in a 75 cm^2 culture flask and maintained in a tissue culture incubator at 37 °C and 5% CO_2 atmosphere. The culture medium was replaced every 2 days. After reaching about 90% confluence, the cells were

detached by 0.025% trypsin and 0.01% EDTA in PBS solution and transferred to a centrifuge tube containing the culture medium. After centrifuging, the cells were re-suspended in fresh culture medium and counted using a Countess™ II Automated Cell Counter (Thermo Fisher Scientific) before seeding to *DS-NNEMs* samples.

Cell seeding in DS-NNEMs: *DS-NNEMs* sample pieces (n=3/sample) were cut in 10 mm diameter and attached in wells of a 24 well plate with Surgical Silicone Adhesive (Kwik-Sil™). The samples were sterilized by placing the well plate under UV light in a sterile fume hood overnight. After sterilization, samples were rinsed with sterile DI water (twice) and 1× DPBS before cell seeding. One milliliter of the Dulbecco's modified Eagle's medium (DMEM) (Life Technologies, Grand Island, NY) supplemented with 10% fetal bovine serum (FBS) and 1% antibiotics (10,000 units/mL of penicillin and 10,000 μg/mL of streptomycin) were added to each well plate and incubated for 3 h before cell seeding. A 50 μL aliquot of medium containing cells (~50,000) was seeded on the *DS-NNEMs* (n = 3) and grown in a humidified incubator (37 °C, 5% CO_2) for specific time points (1, 2, and 3 days).

Cell viability and toxicity analysis: Cell viability of 3T3 fibroblasts with the *DS-NNEMs* and with free drugs was monitored using Alamar Blue (AB) colorimetric assay. The viability of 3T3 cells with the free drug was carried out by adding different concentrations (50, 100, and 200 μg) of free drugs dissolved in cell culture media. See details of drug solution preparation **Supplemental Information SI-2**. Free drug concentrations were selected based upon the loaded drug on DS-NNEMs. At a specific time point, cell culture medium was collected from each *DS-NNEMs/cell* incubated samples and stored for toxicity study. Then the *DS-NNEMs/cell* was washed twice with PBS and incubated for 4 h with 10% (v/v) AB reagent in the respective culture medium. Assay

solutions were transferred to fresh well plates to measure fluorescence (530 nm excitation and 590 nm emission). Cell viability was calculated using the following equation:

$$\text{Cell viability} = \frac{\text{fluorescence of the samples} - \text{fluorescence of the blank}}{\text{fluorescence of the control} - \text{fluorescence of the blank}} \times 100\% \quad (2)$$

Cytotoxicity of *DS-NNEMs* samples was performed using the Pierce LDH assay kit with manufacturer instruction. Briefly, 50 µL of collected sample medium (n=3) was transferred to a flat-bottomed clear 96-well plate and mixed with 50 µL reaction mixture. The plate was covered with aluminum foil and incubated at room temperature for 30 minutes. 50 µL of Stop Solution was added to each well to stop the reaction and the absorbance of the samples was measured at 490 nm and 680 nm by a microplate reader (CLARIOstar Plus, BMG LABTECH Inc., Cary, NC, USA). Cell cytotoxicity was calculated using the following equation:

$$\text{Cytotoxicity (\%)} = \frac{OD_{490nm,\ test\ sample} - OD_{490nm,\ negative\ control}}{OD_{490nm,\ positive\ sample} - OD_{490nm,\ negative\ control}} \times 100\% \quad (3)$$

Fluorescence images of *DS-NNEMs/cell* were performed by staining with acridine orange and propidium iodide (AOPI) dye (Nexcelom Bioscience, Lawrence, MA). At specific time points, cultured media was aspirated from the wells, and *DS-NNEMs/cell* samples were washed with DPBS twice. Then samples were stained with 20 µl dye and incubated at 37 °C for 10 min. Z-stack fluorescence images of *DS-NNEMs/cell* were photographed under an Olympus I×83 microscope using Olympus cell Sens Dimension software (Olympus Corporation, Shinjuku, Tokyo, Japan) where live and dead cells stained as green and red, respectively. Cells were counted (live and dead) from the fluorescence images using ImageJ 1.53c (NIH, Bethesda, MD, USA).

Cell fixation and cell attachment: After the cell cytotoxicity assay, *DS-NNEMs/cell* samples were fixed, and cellular morphology was examined at the SEM. Samples were washed with DPBS twice

and fixed with 4% glutaraldehyde for 30 min. After fixing, samples were rinsed twice with DI water and dehydrated by sequential incubations in 50, 75, and 100% ethanol at room temperature. The sequential wash between the different percent of ethanol was carried out at 10 min-intervals. The samples were left to dry in the sterile fume hood for 24 h and imaged at the SEM.

***Statistics**:* Data are presented as mean ± S.D. Experimental results were analyzed for significance with OriginPro software (Origin Lab, Northampton, MA, USA) using a one-way analysis of variance (ANOVA). The α-value was set to 0.05 and the p-value less than 0.05 was considered statistically significant.

Results

Nanofiber morphology of DS-NNEM: SEM images revealed important differences in fiber morphology of PCL, CH, and PCL-CH (PC-0) (Fig. 1 A, B, and C). PCL and PCL-CH fibers were bead-free, had a smooth surface, and were oriented mostly in a single direction whereas CH fibers showed some branched network of small and large fibers. The fiber morphology of PCL and PCL-CH did not change significantly before and after neutralization and washing with DI water whereas CH fibers were swollen and melted at the fiber overlap points (Fig. 1 A′, B′, and C′). As seen in the fiber diameter distribution graphs in Fig. 1, diameter of PCL fibers varied from 0.25 μm to 3.25 μm with an average value of 1.49 μm (n=50), whereas average diameter values of CH was 0.32 μm (n=50), and PCL-CH was 0.12 μm (n=50). A significant difference (ANOVA, *p=0.05, n=50*) of the average diameter of CH and PCL-CH is observed as compared to PCL fiber.

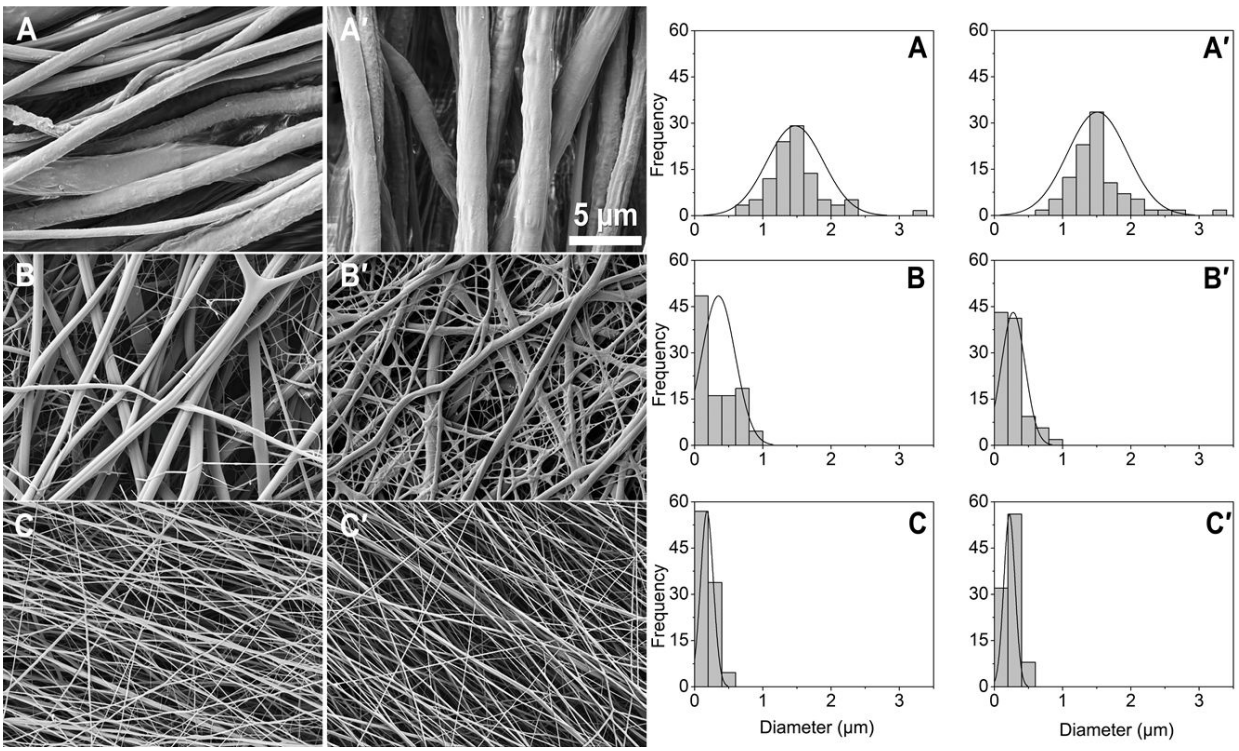

Figure 1. *Surface morphology and diameter distributions of electrospun nanofiber mesh of PCL, CH, and PCL-CH. Left: SEM images of as-prepared PCL (A), CH (B), and PCL-CH (C) nanofiber mesh. Images of A', B', C' are corresponding SEM images of A, B, C after neutralization, and washed with DI water, respectively. Right: Distribution of fiber diameters of as-prepared (A, B, C) and neutralized (A', B', C') mesh measured using Image-Pro Plus 6.0 software.*

SEM images and fiber diameter distribution graphs (Fig. 2) show the surface morphology and diameter distributions of DS-loaded PCL-CH nanofiber meshes, labeled as *DS-NNEMs*. With increasing DS concentration, the morphology of fibers changed drastically, a new secondary phase of nanonet fibers appeared (Fig. 2 A, B, and C). These nanonet fibers were barely visible in PC-4 (4% DS in DS-NNEMs) mesh, whereas their appearance is significant in PC-8 (8% DS in DS-NNEMs) and PC-12 (12% DS in DS-NNEMs) meshes. The morphology of these nanonets was closely observed in high-resolution SEM images; and it appeared that the average diameters of the

new secondary phase fibers were around 0.03 μm (n=100), which was about 7 times smaller than that of the primary nanofibers (average 0.20 μm, n=100). The nanonet structures were intact and visible even after neutralization and washing with DI water (Fig. 2 A′, B′, and C′).

When DS concentration was increased up to 25%, the formation of the secondary phase of nanonet fibers in DS-NNEMs was significantly changed. Distribution of DS in *DS-NNEMs* samples was very heterogeneous and inconsistent from batch to batch. Ample amounts of nanonet fibers with precipitation of the excess DS crystals within the fiber networks were visible in SEM images (Supplemental Figure SF-1). Therefore, only meshes with up to 12% DS were used for further analysis. The distribution of DS within the primary and secondary fibers in *DS-NNEMs* was confirmed by SEM-EDS analysis (Supplemental Figure SF-2 and Table ST-1).

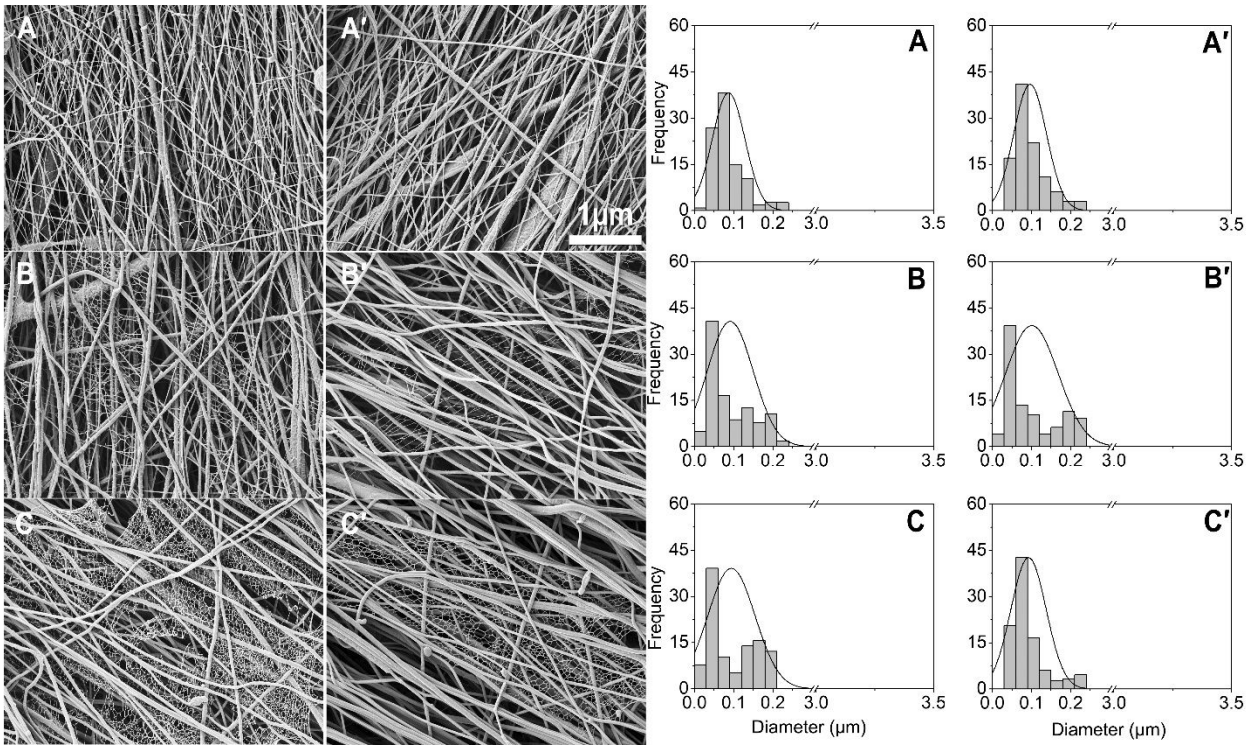

Figure 2. *Surface morphology and diameter distributions of DS-NNEMs (PC-4 to PC-12). Left: SEM images of as-prepared DS-NNEMs samples (PC-4, PC-8, and PC-12). Images of A', B', C'*

are corresponding SEM images of A, B, C after neutralization, and washing with DI water, respectively. Right: Distribution of fiber diameters of as-prepared (A, B, C) and neutralized (A', B', C') mesh measured by using Image-Pro Plus 6.0 software.

FTIR analysis: The FTIR spectra were measured to confirm the presence of different chemical constituents in the *DS-NNEMs* (Fig. 3). Typical absorption bands for PCL nanofiber were located at 1724 cm^{-1} for the stretch of CO in ester groups; 1240 cm^{-1} and 1170 cm^{-1} for C–O–C asymmetric and symmetric stretching vibrations, respectively. These peaks were also present in all other samples with CH and different amounts of drug content. In CH nanofibers, additional peaks were observed at 1533 cm^{-1} and 1662 cm^{-1} corresponding to amine and amide groups of chitosan. These results confirmed the presence of CH in the DS-NNEMs**.** NNEMs loaded with DS showed the characteristic absorption peak at 1575.63 cm^{-1} corresponding to –C═O stretching of carboxyl ion, and 746.86 cm^{-1} corresponding to C–Cl stretching, confirming the presence of DS after series of dissolution and electrospinning process.

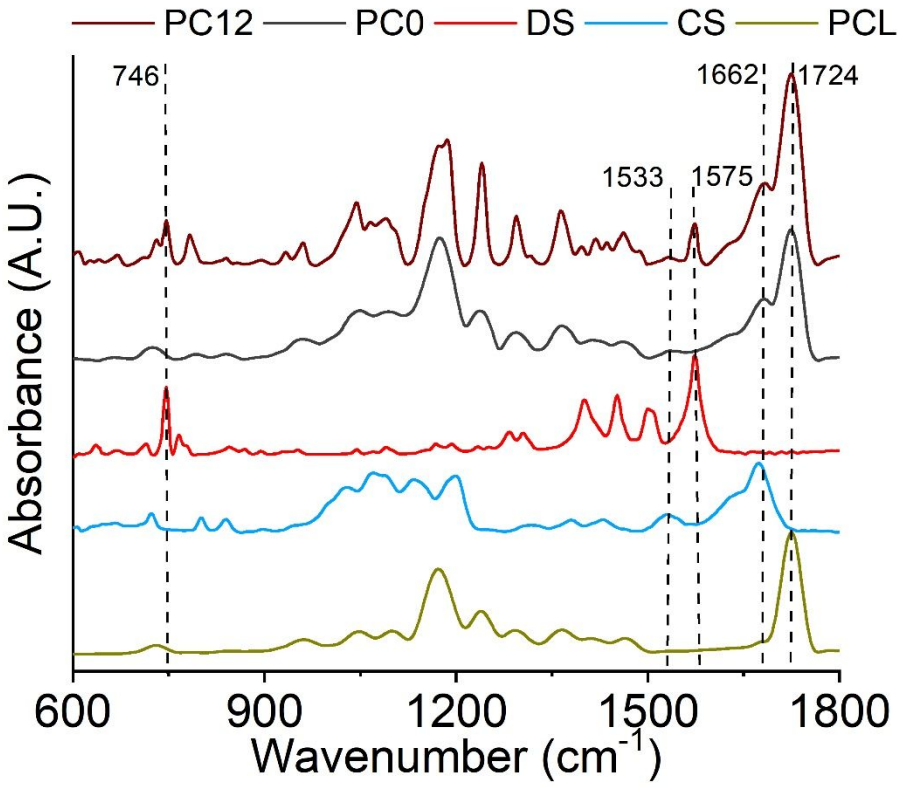

Figure 3. *FTIR spectra of PCL, CH, DS, PC-0, and PC-12. Characteristic absorption peaks at 1662 cm^{-1} and 746 cm^{-1} confirm the presence of CH and DS in the DS-NNEMs nanofiber mesh (i.e. PC-0 and PC-12), respectively. FITR spectra allow comparisons of chemical interactions between PCL, CH, and DS among the DS-NNEMs types.*

Differential scanning calorimetry (DSC)*:* Comparative study of crystallinity and melting temperatures of the *DS-NNEMs* was carried out using DSC analysis (Fig. 4). PCL fiber showed a melting endotherm at 60 °C, which is characteristic of the melting point (T_m) of PCL [50]. T_m of PCL decreased by 3-4^o C in PCL-CH (i.e. PC-0) and *DS-NNEM*s (i.e. PC4-12) samples. Box plots in Fig. 4 represent the variation of the degree of crystallinity of PCL in composite meshes. A significant difference ($p < 0.05$) of the change of PCL crystallinity between PCL and *DS-NNEM*s samples was observed except in PC-0 ($p > 0.05$).

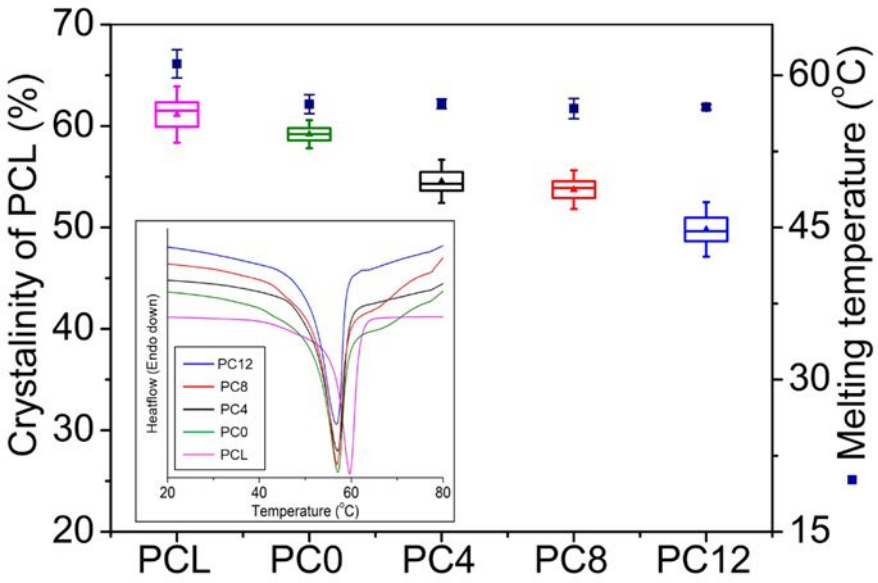

Figure 4. *Crystalline properties of the nanofiber mesh. Box diagrams show changes in crystallinity of PCL whereas line dots show the changes in melting points of without and with DS drug (DS-NNEMs samples; PC-0, PC-4, PC-8, and PC-12) loaded fiber mesh. The inset data shows the representative DSC curves of PCL and DS-NNEMs samples. Averages and standard deviations are given for the analysis of fibers in three meshes (n = 3).*

Mechanical properties: Mechanical properties of the DS-NNEMs samples were assessed via tensile tests. Young's modulus and the tensile strength of nanofiber mesh were measured from strain-stress curves of the samples as the concentration of DS was varied (Fig. 5). The electrospun PCL mesh had an ultimate tensile strength and Young's modulus of 9.7 ± 2 and 34.2 ± 8 MPa, respectively. Mechanical properties summarized in Table 2 show that ultimate tensile strength of DS-NNEMs samples was comparable with PCL mesh whereas Young's modulus is significantly different.

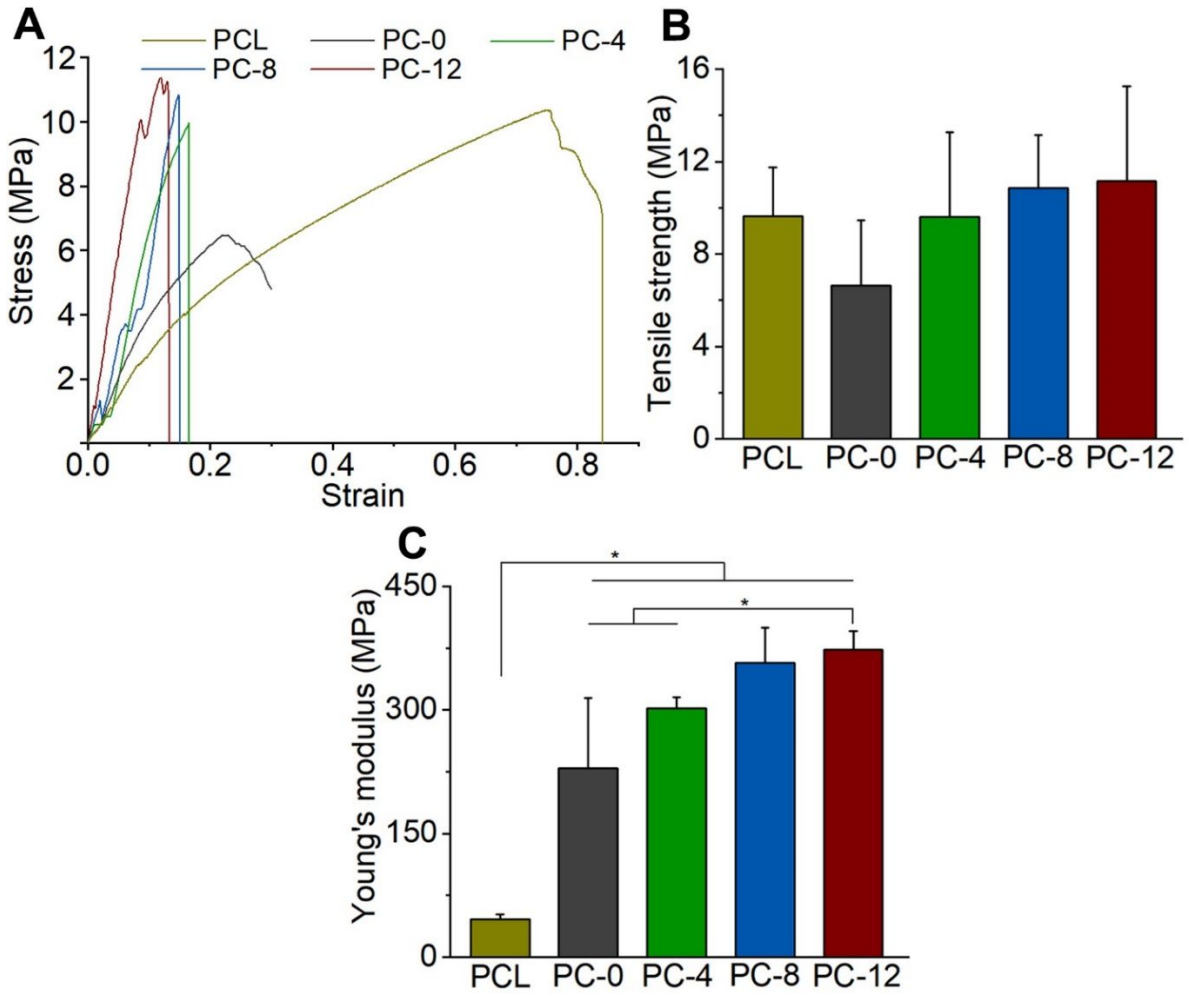

Figure 5. *Mechanical properties of nanofiber mesh samples. (A) Stress-strain curves, showing saw-tooth patterns, (B) Ultimate tensile strength, and (C) Young's Modulus of control PCL fiber and DS-NNEMs experimental samples (PC-0, PC-4, PC-8, and PC-12). ANOVA, p*<0.05. n=5.*

Table 2: Mechanical Properties of PCL and *DS-NNEMs*.

Samples	Tensile Strength (MPa)	Young's Modulus (MPa)
PCL	9.7±2	34.2±8
PC-0	6.6±3	229.2±85
PC-4	9.6±3	302.3±13
PC-8	9.6±3	357.5±42
PC-12	11.1±4	373.1±23

Wettability: Contact angle measurements showed a decrease in angle from 133° for PCL to ~50° for PC-0 mesh sample (Fig. 6). However, initial contact angle measurement for the drug-loaded fibers increased from 49.4° for PC-0 to ~90° for PC-12. Moreover, the contact angle of PCL nanofibers remained constant for 20 secs after droplet formation while water was completely absorbed into DS-NNEMs samples at the same time point.

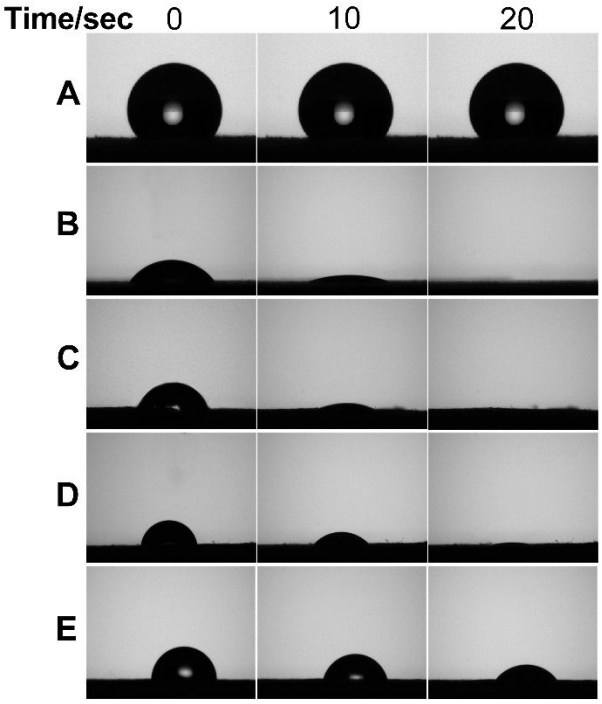

Figure 6. *Wettability study of the* DS-NNEMs*. Images of water-droplets and their contact angles on control PCL sample (A), and DS-NNEMs experimental samples (Images B-E represent PC-0, PC-4, PC-8, and PC-12, respectively).*

Drug release profile: To evaluate DS release characteristics of the DS-loaded mesh; *DS-NNEMs*, *in vitro* dissolution tests, were carried out in DPBS for 14 days at pH 7.4. DS release profiles from

the samples are shown in Fig. 7. No burst release was observed rather than a gradual sharp outcome of DS from PC-4, PC-8, and PC-12 for the first 12 h compared to the release for an extended time (See inset of Fig. 7). PC-4 showed a higher release in percentile (~31%), compared to PC-8 (~27%) and PC-12 (~21%) with the corresponding cumulative release amount of ~317 µg, 600 µg, and 909 µg, respectively, in first 12 h. Gradual release of drug was observed from all DS-NNEMs samples during the entire experimental period. At the end of the experiment (336 h), cumulative release amount for PC-4, PC-8, and PC-12 were approximately 774 µg (75.48%), 1182 µg (52.02%), and 1813 µg (41.75%), respectively.

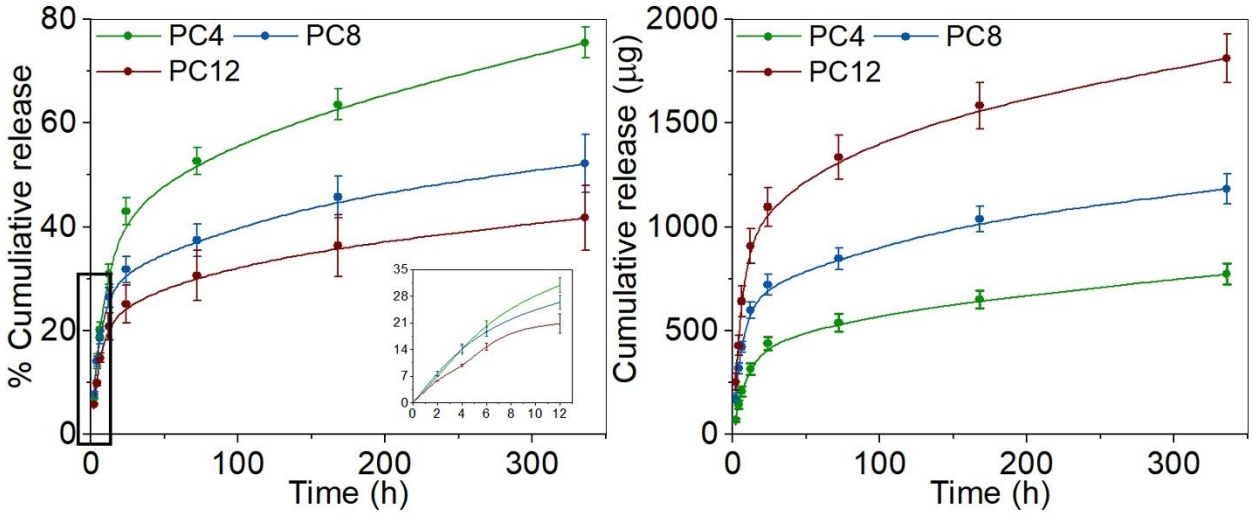

Figure 7. *In vitro DS drug release from DS-NNEMs samples (PC-4, PC-8, and PC-12). Left: Cumulative release (in percentage) of the drug from DS-NNEMs during immersion under phosphate buffer solution over 14 days (336 h). The inset shows the release pattern at the time frame 0-12 h. Right: Cumulative release (in absolute amount) of the drug from DS-NNEMs during immersion under PBS over 14 days (336 h). Data are representative of multiple experiments (n=3).*

Viability and cytotoxicity study*:* Viability and cytotoxicity of 3T3 fibroblast cells grown in samples (PC-0, PC-4, PC-8, and PC-12) were assessed using the standard *in-vitro* assay. Cells

were directly plated on the *DS-NNEMs* and cultured for periods of 1, 2, and 3 days. The cell proliferation assay using Alamer Blue (Fig. 8, left) shows the cell viability remains relatively unchanged in all tested samples compare to control (PC-0). The cytotoxicity of cultured cells on *DS-NNEMs* using LDH assay (Fig. 8, right) also showed a similar trend. The amount of LDH released levels of PC-4, PC-8, and PC-12 was significantly lower than the control at day 1 and 2 *($p < 0.05$)*. There was no significant difference in LDH release among all tested samples on day 3. The viability of 3T3 fibroblast cells grown on PC-0 samples with different concentrations of free drugs (i.e. DS-50 to DS-200 ug/ml) (Fig 8C) was also studied. The viability result of one of the free drugs (i.e. DS-200) was compared with highest drug loaded DS-NNEM samples (i.e. PC-12) (Figure 8D). Test results showed the significant drop of cell viability with free dugs with increasing concentration and exposure time. Cell viability was reduced to 52.6±6% for day 1, and 26.8±5% for day 3 for DS-200. In contrast to free drug, the highest drug-loaded sample (PC-12) showed very insignificant cell viability.

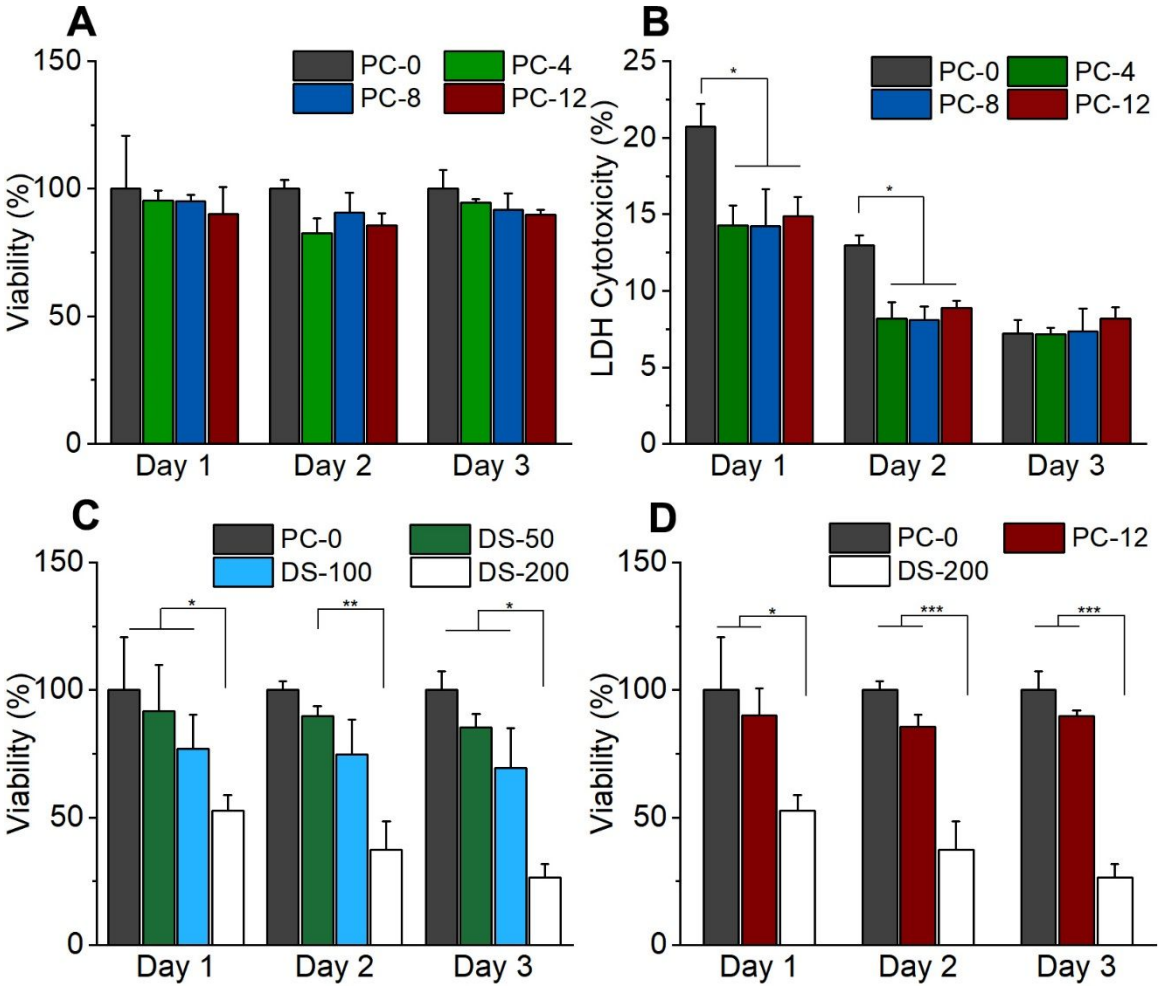

Figure 8. *DS-NNEMs in vitro performance. (A) Cell viability of 3T3 fibroblasts cultured on DS-NNEMs for 1, 2, and 3 days. (B) LDH cytotoxicity of the 3T3 fibroblasts cultured on the DS-NNEMs meshes. (C) Cell viability of 3T3 fibroblasts cultured on PC-0 mesh and exposed with free DS (50, 100 and, 200 µg/mL) for 1, 2, and 3 days. (D) cell viability compared with free drug (DS-200) vs loaded drug on PC-12. All data were normalized to control samples and presented as representative of multiple experiments (n=3). ANOVA, p < 0.05*, p<0.01** and p<.001***.*

Cell attachment, imaging, and counting*:* Cellular biocompatibility including cell adhesion and spreading, as well as cell interactions with nanofibers, were studied using SEM and fluorescence imaging. Fig. 9 (A-D) shows the SEM images of 3T3 cells attached well on *DS-NNEMs* samples

(PC-0, PC-4, PC-8, and PC-12) with their flat shape and sheet-like spreading. Cells projected filopodia along the nanofibers indicating the growth of cultured 3T3 fibroblasts (representative images shown on day 3) were normal. However, the number of attached cells varied among different samples with increased drug concentration. Fig. 9 (E-H) presents representative fluorescent images of cells cultured on *DS-NNEMs* samples, respectively. Live and dead cells were stained green and red color, respectively. Fluorescence images indicated that there was no significant difference in dead cells (red color stained cells) among the tested samples on day 3. Live and dead cells were counted from the fluorescence images by using ImageJ program and the ratio of live to dead cells was plotted (Supplemental Figure SF-3).

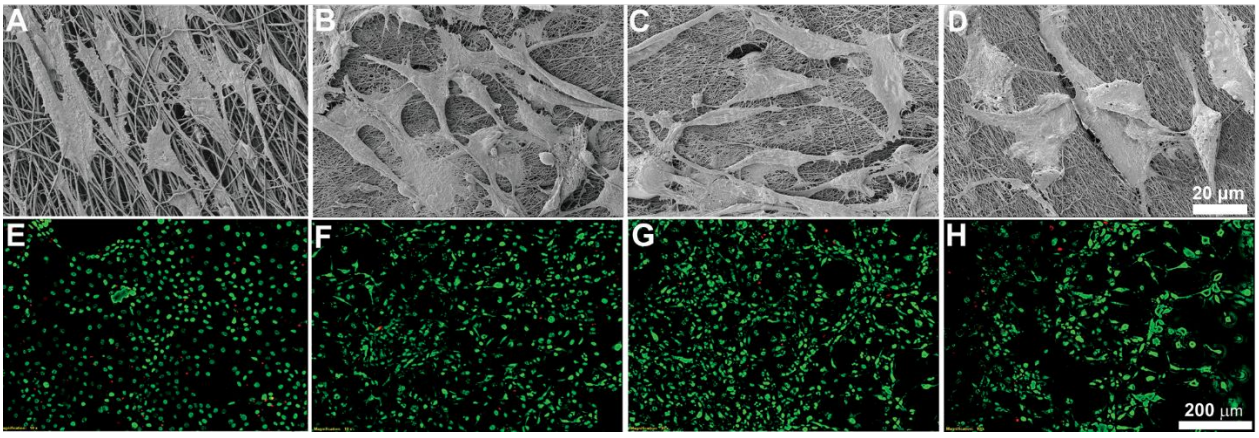

Figure 9. *Cell response in vitro test of DS-NNEMs. SEM Images A to D represents the morphology and attachments of 3T3 fibroblasts cultured for 3 days on DS-NNEMs samples (PC-0, PC-4, PC-8, and PC-12) respectively. Fluorescent microscopy images E to H represent live (stained green) and dead (stained red) 3T3 fibroblasts cultured for 3 days on samples (PC-0, PC-4, PC-8, and PC-12) respectively. Cells were stained with AOPI dye.*

Discussion

NNEM of PCL-CH was prepared by increasing the amount of DS with PCL-CH serving as the control. Individual fibers of PCL and CH were also prepared for comparison study between

DS loaded and unloaded samples. The changed in diameter is probably PCL mesh exhibited larger diameter fibers with the fiber diameter significantly decreasing in PCL-CH. We believe that the decreasing fiber diameter in PCL-CH is due to the decrease in viscosity (Supplemental Figure SF-4) and an increase in conductivity of the blend solution. It is known that highly polar organic acid TFA can increase the conductivity of the solution. TFA is also known for its chain session reaction with PCL [51], which may also contribute to the decrease in viscosity of the PCL-CH blend. Due to these two factors (i.e. viscosity and conductivity), the charge density of the ejected jet increases during electrospinning, which increases the stretching of the jetted PCL-CH solution, resulting in smaller diameter fibers. Furthermore, as-prepared samples (PCL, CH, PCL-CH, and PC-0 to PC-12) attained a slight increase in fiber diameter after the neutralization process. This change is more pronounced in chitosan (CH) based fiber as it is being a hydrophilic polymer, can easily swell in water which may retain after lyophilization [52]. Based on prior work in spider-net formations [26-31] and our studies, we believe that DS to be a major contributing factor in the formation of the secondary phase of the nanonet structures. A possible mechanism for the generation of the secondary phase of nano-net structures is illustrated in Fig. 10**.** DS is an ionic salt; it can easily be ionized when dissolved in the solvent and formed a complex with a cationic polymer. We observed solubility of DS in reverse order of concentration. The higher concentration of DS was more soluble than the lower concentration, an indication of forming complex molecules between DS and chitosan (Supplemental Figure SF-5). We observed more nanonet structures when a higher concentration of DS (i.e. PC-12>PC-8>PC-4) was used. Although the detailed chemistry of this process is beyond the scope of this work, we believe that the charged ions of DS have formed complexes and droplets with the PCL-CH solution. When such a complex mixture is charged under high voltage during electrospinning, the levitating clusters of droplets and complexes undergo

stretching and solvent evaporation. As a result, nanonet structures in the form of spider-nets sandwiched through the main fibers and branched short fibers between the main fibers were formed (Fig. 11).

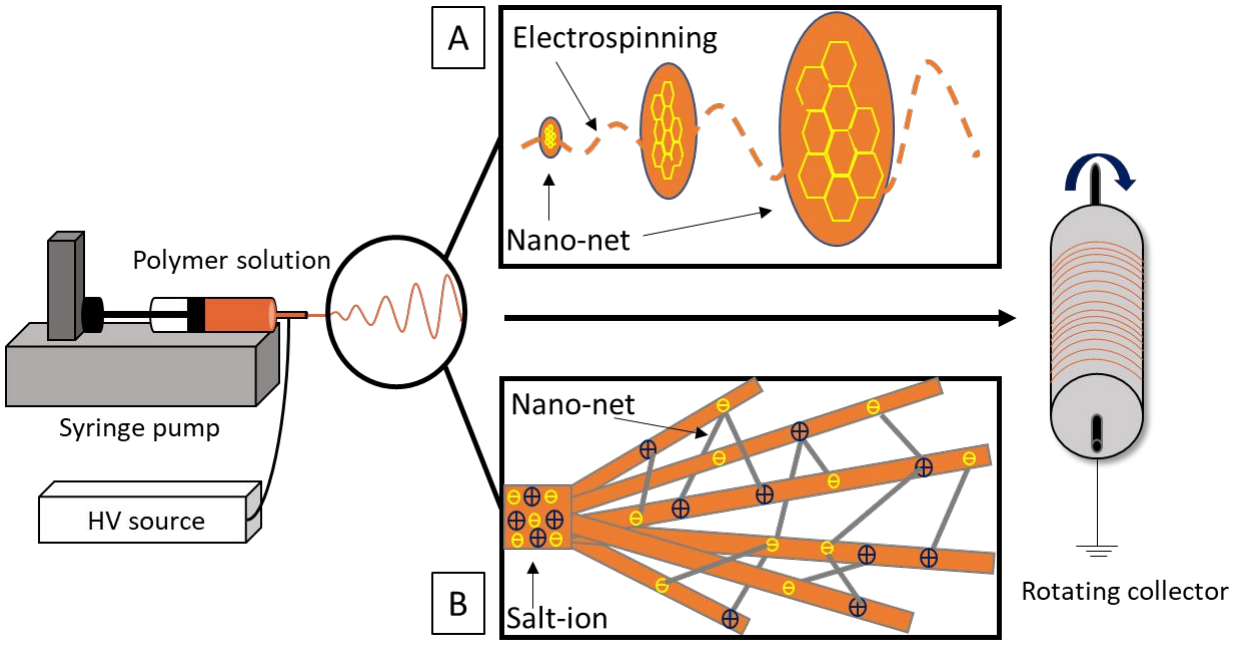

Figure 10. *Schematic illustration of a possible mechanism for nano-net formation during electrospinning (A) charged droplet stretch by applied electric force with phase separation produced spider nets, (B) higher number of free ions of salt distributed through the main fiber produced the branched short fibers.*

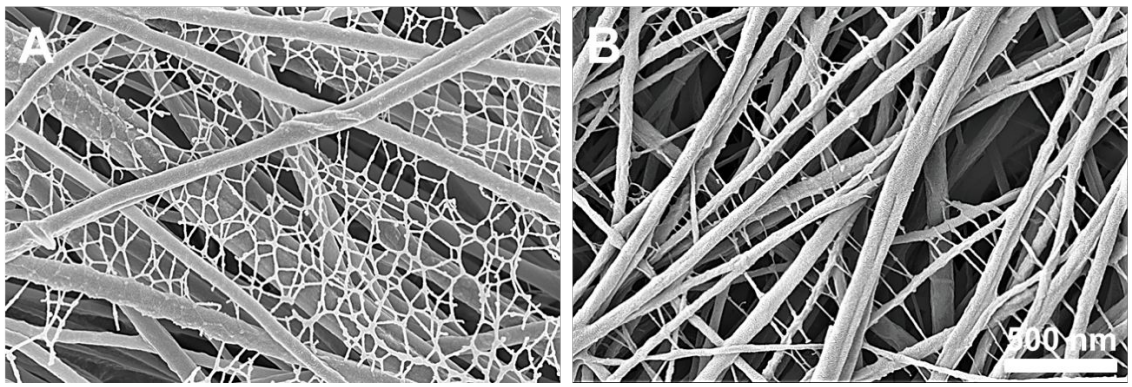

Figure 11. *Nanonet Electrospun Mesh Fiber. (A) Spider-nets with phase separation, (B) branched nano-net produced between the main fibers.*

Using FTIR analysis, whether the presence of DS in NNEMs altered the chemistry of PCL-CH was examined. Several absorption bands in the spectra of PCL, CH, and DS were compared with *DS-NNEM*s. Spectra for *DS-NNEMs* did not show any additional peaks or a significant shift in the characteristic band of individual polymers or drugs, indicating that no covalent bonding between the constituents during NNEMs synthesis.

Following FTIR analysis, DSC was used to further explore the interactions between the drug and the polymer within the polymer matrix. It was reported earlier that melting temperature (T_m) of chitosan appears above its thermal degradation temperature. It is generally difficult to detect the T_m of CH with a conventional DSC instrument [53]. Therefore, only the thermal properties of PCL were measured in the different samples. Even though there was a small decrease in the position of melting endothermic peak, no significant shift of T_m for all PCL-CH fibers with or without the drug was measured. However, the peak area reduced with increasing drug concentration confirming that PCL crystallinity was suppressed significantly by increasing the amount of DS. This reduced crystallinity is likely due to the formation of a lower degree of molecular order in the *DS-NNEMs* fibers primarily caused by their close molecular interactions during the electrospinning process.

Results from mechanical testing showed that DS-loaded NNEMs had significantly higher Young's modulus compared to parent PCL fibers. However, the tensile strength of DS loaded fibers was comparable with PCL. Several regions with sawtooth patterns were observed in the stress-strain curve of drug-loaded samples which implies force was not evenly distributed along

with the fiber. As SEM images of drug-loaded meshes confirm nano-net fiber were not distributed evenly throughout the meshes during the electrospinning process, we assume tensile force during the test was focused on local points where the secondary nanonet-nano fiber was deposited with main fiber. Additionally, the brittle nature of the *DS-NNEMs* compared to PCL fibers could be due to the hydrolytic reaction on PCL polymer with TFA. Such chemical reaction might affect the elastic property of the PCL molecule and result in the blend solution produced near-zero ductile fiber meshes.

Release of DS from DS-NNEM samples was studied for up to 14 days (336 h). All samples showed a biphasic release starting with a sharp release followed by a slow diffusion-controlled release. The sharp outcome was observed within the first 12 h with the highest release rate in PC-4 compared to the other two samples. DS release increased after this time point until reaching saturation. At the end of day 14, the highest amount of DS, as a percentile, was also released from PC-4. As mentioned earlier, a higher amount of DS in solvent showed higher solubility, and a higher percentage of DS resulted in a higher amount of nano-net structures during electrospinning. We assumed the higher percentage of nanonet structures contributing to the slow release rate in PC8 and PC12 compared to PC4. More studies are needed to further understand the underlying mechanism of action and the DS release profile.

The biocompatibility of DS-NNEMs samples and free drug toxicity was carried out by culturing NIH 3T3 cells for up to 3 days. It was reported that the growth of fibroblast cells inhibits when exposed to DS [46, 47]. Al-Nimer et al. has reported that DS inhibits the growth of 3T3 cells up to 75% within the first 24 h. Additionally, Giuri et al. showed that more than half of the initial cell viability reduced in the first 24 h which reached one-third after 48 h. The toxicity data reported by both groups was done by using the free DS of 625 μg and 105 μg, respectively. However, when

the drug was encapsulated within hybrid-nanofiber, the toxicity was reduced and viability increased up 85% in 24 h and 63% in 48 h [47]. In our study, the highest concentration of DS used for cell toxicity study was in PC-12 samples, approximately 200 μg. We compared the cell viability results both the highest drugs loaded sample (PC-12) with an equivalent amount of free drug (DS-200). Our free drug test results showed a similar trend which is consistent with the earlier published report. As no significant differences in cell viability were observed in the DS-NNEMs samples compared to the control, we concluded that, by releasing the drug in a controlled manner, our DS-NNEMs samples showed no adverse effect on cells up to day 3. Additionally, all DS-NNEMs samples showed more than 75% viability, indicating no toxicity of DS-NNEMs mesh for safe use in biomedical applications, according to current ISO standards (ISO-10993-5) [54]. The LDH cytotoxicity data also showed a similar trend supporting the cell viability results. Ratio of live cells to dead cells from the fluorescence images indicating insignificant cells were dying in test samples compared to the control group. The cell-matrix interactions were further studied with SEM images of cells on DS-NNEMs after day 3. The cell morphology reveals that filopodia grew from the cells and attached itself along fiber direction, indicating favorable cell-growth and migration conditions for the cells in DS-NNEM.

Conclusion

In this study, we synthesized diclofenac sodium (DS) contained nanonet-nanofiber electrospun mesh (DS-NNEM) of polycaprolactone (PCL)-chitosan (CH) using electrospinning technology. The objective was to use NNEMs for high payload and controlled release of the water-soluble drug, DS. The results show that incorporating DS with higher concentration played a major role in the formation of secondary phases of ultrafine nanonet structures along with primary nanofibers of PCL-CH. The surface morphology and aqueous stability, distribution of drug

molecules of NNEMs were analyzed. The incorporation of DS caused no changes in the chemical structure of PCL and CH but changed the crystallinity and mechanical properties of the fibers. Drug loading and release data supported prolonged and sustained release from DS-NNEMs. Because of the very slow degradation of nanofiber mats, we believe that DS is released either by diffusion or by permeation through DS-NNEMs structure. The cell viability and imaging data indicate that NIH 3T3 cells experienced no toxicity in the DS-NNEMs structure. In summary, the results suggest that NNEMs technology can potentially serve as a biomimetic platform for loading and sustained release of biologically active therapeutic compounds and other drugs for prolonged periods.

Acknowledgments

This work was supported financially by the National Science Foundation, through the Engineering Research Center for Revolutionizing Metallic Biomaterials (ERC-RMB, EEC-0812348). We thank Dr. Salil Desai's lab, North Carolina A&T State University, for their technical assistance to measure viscosity. Characterization of DS-NNEMs was performed in part at the Joint School of Nanoscience and Nanoengineering, a member of the Southeastern Nanotechnology Infrastructure Corridor and National Nanotechnology Coordinated Infrastructure (NSF ECCS-1542174).

References

1. Gopal, R., et al., *Electrospun nanofibrous filtration membrane.* Journal of Membrane Science, 2006. **281**(1-2): p. 581-586.

2. Aussawasathien, D., C. Teerawattananon, and A. Vongachariya, *Separation of micron to sub-micron particles from water: Electrospun nylon-6 nanofibrous membranes as pre-filters.* Journal of Membrane Science, 2008. **315**(1-2): p. 11-19.
3. Schreuder-Gibson, H., et al., *Protective textile materials based on electrospun nanofibers.* Journal of Advanced Materials, 2002. **34**(3): p. 44-55.
4. Lee, S. and S.K. Obendorf, *Developing protective textile materials as barriers to liquid penetration using melt-electrospinning.* Journal of Applied Polymer Science, 2006. **102**(4): p. 3430-3437.
5. Gorji, M., A.A.A. Jeddi, and A.A. Gharehaghaji, *Fabrication and characterization of polyurethane electrospun nanofiber membranes for protective clothing applications.* Journal of Applied Polymer Science, 2012. **125**(5): p. 4135-4141.
6. Rojas, R. and N.J. Pinto, *Using electrospinning for the fabrication of rapid response gas sensors based on conducting polymer nanowires.* Ieee Sensors Journal, 2008. **8**(5-6): p. 951-953.
7. Kowalczyk, T., et al., *Electrospinning of bovine serum albumin. Optimization and the use for production of biosensors.* Biomacromolecules, 2008. **9**(7): p. 2087-2090.
8. Dong, Z.X., S.J. Kennedy, and Y.Q. Wu, *Electrospinning materials for energy-related applications and devices.* Journal of Power Sources, 2011. **196**(11): p. 4886-4904.
9. Bhattarai, N. and M. Zhang, *Controlled synthesis and structural stability of alginate-based nanofibers.* Nanotechnology, 2007. **18**(45): p. 455601.
10. Edwards, A., et al., *Poly (ε-caprolactone)/keratin-based composite nanofibers for biomedical applications.* Journal of Biomedical Materials Research Part B: Applied Biomaterials, 2015. **103**(1): p. 21-30.
11. Bhattarai, N., et al., *Natural-Synthetic Polyblend Nanofibers for Biomedical Applications.* Advanced Materials, 2009. **21**(27): p. 2792-+.
12. Cooper, A., et al., *Aligned chitosan-based nanofibers for enhanced myogenesis.* Journal of materials chemistry, 2010. **20**(40): p. 8904-8911.
13. Bhattarai, S.R., et al., *Novel biodegradable electrospun membrane: scaffold for tissue engineering.* Biomaterials, 2004. **25**(13): p. 2595-2602.
14. Khil, M.S., et al., *Novel fabricated matrix via electrospinning for tissue engineering.* Journal of Biomedical Materials Research Part B: Applied Biomaterials: An Official

Journal of The Society for Biomaterials, The Japanese Society for Biomaterials, and The Australian Society for Biomaterials and the Korean Society for Biomaterials, 2005. **72**(1): p. 117-124.

15. Bajgai, M.P., et al., *Poly (ϵ-caprolactone) grafted dextran biodegradable electrospun matrix: A novel scaffold for tissue engineering.* Journal of Applied Polymer Science, 2008. **108**(3): p. 1447-1454.
16. Cooper, A., N. Bhattarai, and M.Q. Zhang, *Fabrication and cellular compatibility of aligned chitosan-PCL fibers for nerve tissue regeneration.* Carbohydrate Polymers, 2011. **85**(1): p. 149-156.
17. Bhattarai, S.R., et al., *Hydrophilic nanofibrous structure of polylactide; fabrication and cell affinity.* Journal of Biomedical Materials Research Part A: An Official Journal of The Society for Biomaterials, The Japanese Society for Biomaterials, and The Australian Society for Biomaterials and the Korean Society for Biomaterials, 2006. **78**(2): p. 247-257.
18. Khil, M.S., et al., *Electrospun nanofibrous polyurethane membrane as wound dressing.* Journal of Biomedical Materials Research Part B: Applied Biomaterials: An Official Journal of The Society for Biomaterials, The Japanese Society for Biomaterials, and The Australian Society for Biomaterials and the Korean Society for Biomaterials, 2003. **67**(2): p. 675-679.
19. Cooper, A., N. Bhattarai, and M. Zhang, *Fabrication and cellular compatibility of aligned chitosan–PCL fibers for nerve tissue regeneration.* Carbohydrate Polymers, 2011. **85**(1): p. 149-156.
20. Pelipenko, J., P. Kocbek, and J. Kristl, *Critical attributes of nanofibers: Preparation, drug loading, and tissue regeneration.* International Journal of Pharmaceutics, 2015. **484**(1-2): p. 57-74.
21. Bhattarai, N., et al., *Electrospun chitosan-based nanofibers and their cellular compatibility.* Biomaterials, 2005. **26**(31): p. 6176-6184.
22. Kelner, A. and E.H. Schacht, *Tailor-made polymers for local drug delivery: Release of macromolecular model drugs from biodegradable hydrogels based on poly(ethylene oxide).* Journal of Controlled Release, 2005. **101**(1-3): p. 13-20.
23. Lambert, G., E. Fattal, and P. Couvreur, *Nanoparticulate systems for the delivery of antisense oligonucleotides.* Advanced Drug Delivery Reviews, 2001. **47**(1): p. 99-112.

24. Zupancic, S., et al., *Contribution of Nanotechnology to Improved Treatment of Periodontal Disease.* Current Pharmaceutical Design, 2015. **21**(22): p. 3257-3271.
25. Calvino-Casilda, V., et al., *The role of metallic modifiers of SBA-15 supports for propyl-amines on activity and selectivity in the Knoevenagel reactions.* Microporous and Mesoporous Materials, 2016. **224**: p. 201-207.
26. Wang, X., et al., *Electro-spinning/netting: A strategy for the fabrication of three-dimensional polymer nano-fiber/nets.* Progress in Materials Science, 2013. **58**(8): p. 1173-1243.
27. Zhang, S., et al., *Direct electronetting of high-performance membranes based on self-assembled 2D nanoarchitectured networks.* Nature communications, 2019. **10**(1): p. 1-11.
28. Zhang, S., et al., *Tailoring mechanically robust poly (m-phenylene isophthalamide) nanofiber/nets for ultrathin high-efficiency air filter.* Scientific reports, 2017. **7**: p. 40550.
29. Barakat, N.A.M., et al., *Spider-net within the N6, PVA and PU electrospun nanofiber mats using salt addition: Novel strategy in the electrospinning process.* Polymer, 2009. **50**(18): p. 4389-4396.
30. Pant, B., M. Park, and S.J. Park, *One-Step Synthesis of Silver Nanoparticles Embedded Polyurethane Nano-Fiber/Net Structured Membrane as an Effective Antibacterial Medium.* Polymers, 2019. **11**(7).
31. Parajuli, D.C., et al., *Synchronized Polymerization and Fabrication of Poly(acrylic acid) and Nylon Hybrid Mats in Electrospinning.* Acs Applied Materials & Interfaces, 2009. **1**(4): p. 750-757.
32. Warner, T.D., et al., *Influence of plasma protein on the potencies of inhibitors of cyclooxygenase-1 and-2.* Faseb Journal, 2006. **20**(1): p. 542-+.
33. Brogden, R.N., et al., *Diclofenac Sodium - a Review of Its Pharmacological Properties and Therapeutic Use in Rheumatic Diseases and Pain of Varying Origin.* Drugs, 1980. **20**(1): p. 24-48.
34. Hart, F.D. and E.C. Huskisson, *Non-Steroidal Anti-Inflammatory Drugs - Current Status and Rational Therapeutic Use.* Drugs, 1984. **27**(3): p. 232-255.
35. Wan, Y., et al., *Compressive mechanical properties and biodegradability of porous poly(caprolactone)/chitosan scaffolds.* Polymer Degradation and Stability, 2008. **93**(10): p. 1736-1741.

36. Wu, C.S., *A comparison of the structure, thermal properties, and biodegradability of polycaprolactone/chitosan and acrylic acid grafted polycaprolactone/chitosan.* Polymer, 2005. **46**(1): p. 147-155.
37. Van der Schueren, L., et al., *Polycaprolactone and polycaprolactone/chitosan nanofibres functionalised with the pH-sensitive dye Nitrazine Yellow.* Carbohydrate Polymers, 2013. **91**(1): p. 284-293.
38. Sarasam, A. and S.V. Madihally, *Characterization of chitosan-polycaprolactone blends for tissue engineering applications.* Biomaterials, 2005. **26**(27): p. 5500-5508.
39. Neves, S.C., et al., *Chitosan/Poly(epsilon-caprolactone) blend scaffolds for cartilage repair.* Biomaterials, 2011. **32**(4): p. 1068-1079.
40. Wan, Y., et al., *Development of polycaprolactone/chitosan blend porous scaffolds.* Journal of Materials Science-Materials in Medicine, 2009. **20**(3): p. 719-724.
41. Allen, C., et al., *Polycaprolactone-b-poly(ethylene oxide) copolymer micelles as a delivery vehicle for dihydrotestosterone.* Journal of Controlled Release, 2000. **63**(3): p. 275-286.
42. Cai, Q., J.Z. Bei, and S.G. Wang, *Synthesis and degradation of a tri-component copolymer derived from glycolide, L-lactide, and epsilon-caprolactone.* Journal of Biomaterials Science-Polymer Edition, 2000. **11**(3): p. 273-288.
43. Hubbell, D.S. and S.L. Cooper, *Physical-Properties and Morphology of Poly-Epsilon-Caprolactone Polymer Blends.* Journal of Applied Polymer Science, 1977. **21**(11): p. 3035-3061.
44. Zhu, K.J., X.Z. Lin, and S.L. Yang, *Preparation, Characterization, and Properties of Polylactide (Pla) Poly(Ethylene Glycol) (Peg) Copolymers - a Potential-Drug Carrier.* Journal of Applied Polymer Science, 1990. **39**(1): p. 1-9.
45. Cao, H.Q., T. Liu, and S.Y. Chew, *The application of nanofibrous scaffolds in neural tissue engineering.* Advanced Drug Delivery Reviews, 2009. **61**(12): p. 1055-1064.
46. Al-Nimer, M.S., H.G. Hameed, and M.M. Mahmood, *Antiproliferative effects of aspirin and diclofenac against the growth of cancer and fibroblast cells: in vitro comparative study.* Saudi Pharmaceutical Journal, 2015. 23(5): p. 483-486.
47. Giuri, D., et al., *Nano-hybrid electrospun non-woven mats made of wool keratin and hydrotalcites as potential bio-active wound dressings.* Nanoscale, 2019. 11(13): p. 6422-6430.

48. Adhikari, U., et al., *Embedding magnesium metallic particles in polycaprolactone nanofiber mesh improves applicability for biomedical applications.* Acta biomaterialia, 2019. **98**: p. 215-234.
49. Patrício, T. and P. Bártolo, *Thermal stability of PCL/PLA blends produced by physical blending process.* Procedia Engineering, 2013. **59**: p. 292-297.
50. Crescenzi, V., et al., *Thermodynamics of fusion of poly-β-propiolactone and poly-ϵ-caprolactone. comparative analysis of the melting of aliphatic polylactone and polyester chains.* European Polymer Journal, 1972. **8**(3): p. 449-463.
51. Mahoney, C., et al., *Electrospun nanofibers of poly (ε-caprolactone)/depolymerized chitosan for respiratory tissue engineering applications.* Journal of Biomaterials Science, Polymer Edition, 2016. **27**(7): p. 611-625.
52. Mengistu Lemma, S., F. Bossard, and M. Rinaudo, *Preparation of pure and stable chitosan nanofibers by electrospinning in the presence of poly (ethylene oxide).* International journal of molecular sciences, 2016. 17(11): p. 1790.
53. Malheiro, V.N., et al., *New poly (ε-caprolactone)/chitosan blend fibers for tissue engineering applications.* Acta Biomaterialia, 2010. **6**(2): p. 418-428.
54. Wang, J., et al., *Recommendation for modifying current cytotoxicity testing standards for biodegradable magnesium-based materials.* Acta biomaterialia, 2015. **21**: p. 237-249.

Drug-induced nanonet-nano fiber mesh of PCL-chitosan for high entrapment capacity and extended release of hydrophilic drug